Automatic Crater Detection and Age Estimation for Mare Regions on the Lunar Surface

Atheer L. Salih, Philipp Schulte, Arne Grumpe, Christian Wöhler
Image Analysis Group
TU Dortmund
D-44227 Dortmund, Germany
Email: atheer.altameemi@tu-dortmund.de

Harald Hiesinger
Institut für Planetologie
Westfälische Wilhelms-Universität
48149 Münster, Germany

***Abstract*—In this paper, we investigate how well an automatic crater detection algorithm is suitable to determine the surface age of different lunar regions. A template-based crater detection algorithm is used to analyze image data under known illumination conditions. For this purpose, artificially illuminated crater templates are used to detect and count craters and their diameters in the areas under investigation. The automatic detection results are used to obtain the crater size-frequency distribution (CSFD) for the examined areas, which is then used for estimating the absolute model age (AMA) of the surface. The main focus of this work is to find out whether there exists an ideal sensitivity value for automatic crater detection to obtain smallest possible errors between the automatically derived AMA and a reference AMA derived from manually detected craters. The detection sensitivity threshold of our crater detection algorithm (CDA) is calibrated based on five different regions in Mare Cognitum on the Moon such that the age inferred from the manual crater counts corresponds to the age inferred from the CDA results. The obtained best detection threshold value is used to apply the CDA algorithm to another five regions in the lunar Oceanus Procellarum region. The accuracy of the method is examined by comparing the calculated AMAs with the manually determined ones from the literature. It is shown that the automatic age estimation yields AMA values that are generally consistent with the reference values with respect to the one standard deviation errors.**

***Keywords*—remote sensing; automatic crater detection; crater statistics; absolute model age; age mapping.**

I. INTRODUCTION

The age of a planetary surface is of major importance for its subdivision into different geological units and the analysis of volcanic processes. There exists a well-established statistical approach for the estimation of the surface age that relies on the impact crater size-frequency distribution (CSFD) [1].

The absolute age of a planetary surface can be determined by means of radiometric methods, which, however require the acquisition and possibly also the return of surface samples. In contrast, the most practical methods for age estimation are those that do not involve sampling of the surface. They rely on the general observation that the amount of craters increases with the time that has passed since the surface has been deposited. The extracted information regarding the crater rate per area may be directly used to derive the relative age of different planetary surface areas. The main advantage of the crater-based methods is that the required information may be extracted from images and or digital elevation models (DEM). The information is thus extracted only from remotely obtainable data of the surface.

In order to infer absolute model ages (AMA) of the surface, the methods are combined, i.e. the CSFD of areas for which samples are available is determined and then calibrated with respect to the absolute age of the sample. This calibration allows for the estimation of absolute ages of individual areas on the Moon [1].The advantage of performing this procedure through applying an automatic crater detection algorithm (CDA) is the possibility to calculate the AMAs for large areas on a planet much faster than a human could do [2].

Usually, the estimation of the CSFD is done by manually counting craters and determining their size in the available planetary images. Since the AMA highly depends on the CSFD, it is very important to detect all craters and to not include false detections into the CSFD. Although this manual process is highly demanding and time consuming for large areas, it is still preferred over automatic crater detection algorithm, which often miss some craters and/or falsely detect craters. The automatic detection algorithms, however, operate comparably fast and may thus be easily applied to large high-resolution global image mosaics of various planetary surfaces.

A large variety of automated CDAs relying on images or topographic maps of planetary surfaces have been developed recently [3]. Since the AMA is derived from the CSFD using a statistical approach, however, we expect the AMA to be robust with respect to small fluctuations, e.g. false detections or missing detections, in the estimated CSFD. Consequently, this work aims at the estimation of the accuracy of a CDA with respect to the AMA and not with respect to the true and false detections.

II. TEMPLATE MATCHING AND AUTOMATIC CRATER DETECTION

A DEM represents a height profile which is usually generated by means of laser scanning or by stereo image analysis methods. In laser scanning, a satellite equipped with a

ISBN 978-0-9928626-7-1

laser altimeter scans the surface with laser pulses and determines the distance to the surface based on their time of flight, while in stereo image analysis an algorithm generates a DEM based on two or more images of the surface [4].

In remote sensing, the development of image-based CDAs for automatic determination of crater locations and diameters is an important research approach [2, 5]. Knowledge about the impact crater distribution is of high relevance for geologic planetary surface studies performed by remote sensing [3]. In this study a CDA is applied to dark and flat mare regions on the lunar nearside in order to obtain AMA values based on crater counts which have a similar accuracy to those inferred from manual crater counts.

III. CSFD-Based Surface Age Estimation

According to previous studies, the volcanic activity on the Moon has been high in the period of time between 1.2 to 4 billion years (Ga) ago [6]. These activities and eruptions formed a large variety of lunar mare basalt units in different areas. Fig. 1 shows the primary mare areas on the lunar nearside. For the study of lunar volcanic processes, it is very important to know the temporal sequence of individual volcanic activities and how they affect the extents of the corresponding basalt areas.

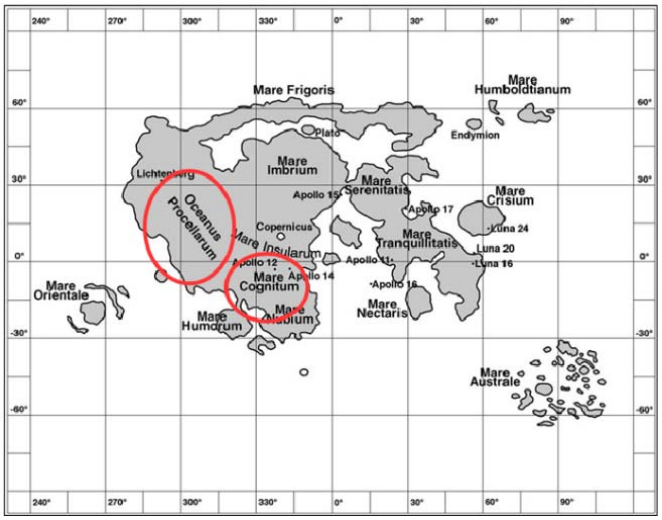

Fig. 1. Mare regions on the lunar nearside (from [6]).

Basically, the AMA estimation process is based on the CSFD which represents the number of craters per diameter interval per unit area. The sensitivity of the applied CDA is controlled by a sensitivity threshold value. This value needs to be adjusted according to the AMA of a reference area obtained manual crater counts. The obtained AMA should be the same as the manually determined AMA. The detected craters allow for constructing the CSFD, represented by a cumulative histogram defined by diameter bins. The user-defined diameter range depends on the image resolution, the crater types and sizes and the craters density per surface area. The so-called production function as e.g. given in [7] is then fitted to the cumulative histogram. It yields the number of craters smaller than a given diameter value per unit area. Then the value $N(d_r)$ of the production function for a reference diameter d_r, where typically d_r=1 km, is determined [7]. A second important function, the chronology function, describes the number $N(1)$ of craters less than 1 km diameter per unit area in dependence of the AMA. Hence, the AMA can be obtained by inversion of the chronology function [7]. Details about the method of CSFD-based AMA estimation are given e.g. in [1, 7]. Typically, determination of the CSFD is performed based on orbital imagery.

IV. Automatic Crater Detection

The CDA utilized in this study relies on cross-correlation based template matching. It examines the similarity between the original image and a set of crater templates at each pixel position. It can be considered as a reliable yet simple method to automatically detect craters in orbital images of the lunar surface. Since CDAs commonly have a parameter that defines their sensitivity, it is important to calibrate this threshold based on a small reference area provided with its manual crater counts [8].

The determination of the CSFD is the main approach to estimate the AMA for various individual geologic regions on the Moon [7]. We derive the CSFD from a mosaic of Wide Angle Camera (WAC) images of the Lunar Reconnaissance Orbiter Camera (LROC) [9]. The spatial resolution of the mosaic is about 100 m per pixel (http://wms.lroc.asu.edu/lroc/view_rdr/WAC_GLOBAL). We assume that the craters can be detected if their diameter equals or exceeds 300 m (3 pixels in the image).

In order to be able to detect craters using the template matching method, we apply the method of [10] and use their six artificially generated 3D crater templates. These 3D models were generated from three different Lunar Orbiter Laser Altimeter (LOLA) profiles [11] through lunar craters of about 8 km diameter. For this purpose, each profile was cut in half at the crater center and then rotated, respectively, to produce six representative 3D crater models as shown in Fig. 2.

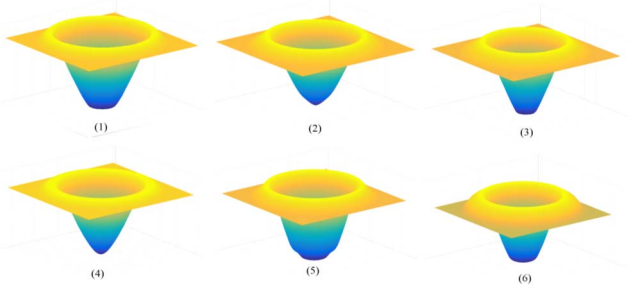

Fig. 2. Utilised set of 3D crater models.

Since the appearance of craters highly depends on the illumination conditions, we use a reflectance model to shade the 3D models of the craters and project the shaded 3D models into a pinhole camera yielding image templates. To estimate the illumination angle of the study part of the WAC mosaic, the GLD100 topographic map [12] of the same area has been artificially illuminated by applying Hapke's reflectance model [13, 14]. The illumination direction was automatically adjusted using a quasi-Newton method in order to maximize the similarity between the WAC mosaic part and the shaded

ISBN 978-0-9928626-7-1 © EURASIP 2017

GLD100. The inferred illumination direction is used to compute the crater image templates.

The generated crater templates are then scaled to a given diameter range of 0.3-20 km and the normalized cross-correlation with the image is computed, respectively, where local maxima of the normalized cross-correlation are set to be crater candidates. Based on a specified threshold value, the determined cross-correlation value indicates whether or not the detected candidate is a crater. Since the same crater may be found by multiple templates and diameters, a fusion procedure is applied to the detected candidates such that multiple detections are removed and a unique diameter value can be determined. In case of several templates corresponding to different crater diameters, the diameter values are averaged to obtain the final diameter.

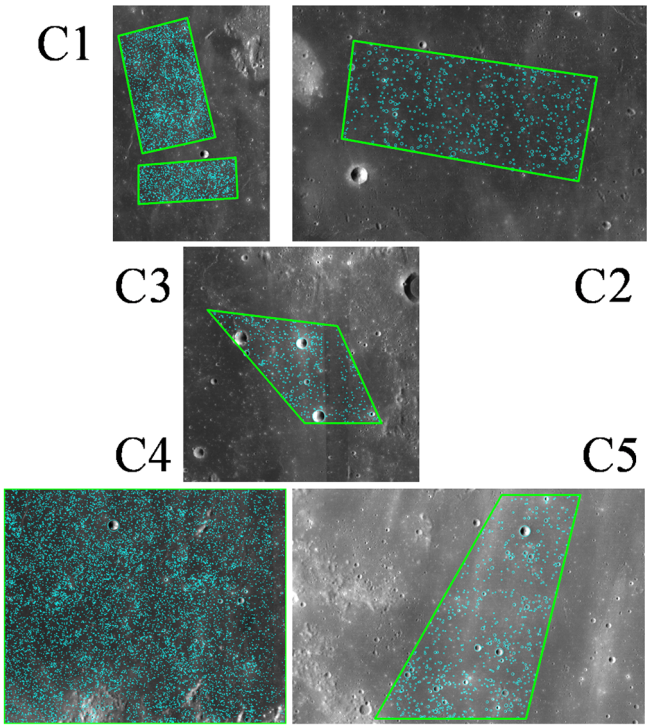

Fig. 3. Craters detected in the counting areas by the template matching based CDA in areas C1-C5. The green polygons denote the counting areas.

The determined crater positions and diameters are then used to derive the CSFD for the study region. This study focuses on the five areas C1-C5 defined in [6] located in Mare Cognitum and another five areas P5, P41, P49, P50 and P51 defined in [6] located in Oceanus Procellarum. All ten study areas are located in a latitude range between 15° S and 30° N and in a longitude range between 285° E and 345° E. Fig. 3 shows the obtained craters for the five study areas C1-C5 located in Mare Cognitum by applying the described template matching based CDA. We adapted the sensitivity threshold of the template matching such that the squared difference between the AMA inferred for C1-C5 and the AMA given in [6] is minimized. Fig. 4 shows the detected craters for the other five study areas P4, P41, P49, P50 and P51 located in Oceanus Procellarum by applying the described template matching based CDA with respect to the optimal threshold obtained for the Mare Cognitum test areas.

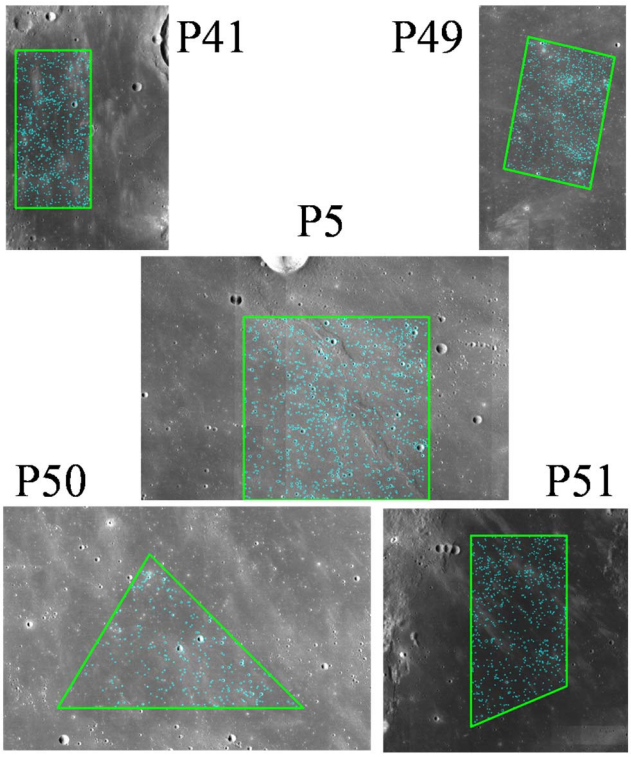

Fig. 4. Craters detected in the counting areas by the template matching based CDA in Oceanus Procellarum areas.The green polygons denote the counting areas.

V. Results and Discussion

Firstly, the optimal cross-correlation thresholds for the regions C1-C5 were calculated automatically by comparing the CDA-based AMAs with the referenced AMAs from [6]. All obtained threshold values are shown in Table 1.

TABLE I. Calibrated detection threshold values for the individual regions C1-C5 in Mare Cognitum.

Area	Calibrated threshold
C1	0.6637
C2	0.6455
C3	0.6541
C4	0.6677
C5	0.6648
Average value	**0.6592**

The arithmetic mean of the five calibrated threshold values amounts to 0.6592. Area C1 consists of two polygons for the crater counting. The other investigated areas have always been defined by a single polygonal shape. By applying this "optimal" threshold value to the areas C1-C5 in Mare Cognitum yields the AMAs listed in Table 2, where they are compared to the reference AMAs from [6] obtained based on manual crater counts. For area C5, there are two reference AMAs given which are interpreted as the result of a resurfacing process in [6].

ISBN 978-0-9928626-7-1 © EURASIP 2017

TABLE II. CDA-BASED AND REFERENCE AMAS FOR THE STUDY AREAS IN MARE COGNITUM AFTER APPLYING THE OPTIMAL DETECTION THRESHOLD.

Area	CDA-based AMA [Ga]			Reference AMA [Ga] [6]		
C1	3.52	-0.008	+0.007	3.49	-0.10	+0.08
C2	3.46	-0.004	+0.004	3.45	-0.06	+0.09
C3	3.63	-0.024	+0.018	3.41	-0.08	+0.08
C4	3.43	-0.002	+0.002	3.36	-0.11	+0.10
C5	3.52	-0.006	+0.005	3.32 3.65	-0.14 -0.08	+0.10 +0.08

The CDA faces difficulties if the illumination direction is different in different image parts, as in area C3. Since the target image is a mosaic, this might occur if images acquired under different illumination conditions are combined. The western half of the image (left of the yellow dividing line) is illuminated from the east while the eastern half is illuminated from the western side as shown in Fig. 5. This causes the illumination vector to be erroneously calculated since our algorithm assumes that the images are homogeneously illuminated from one direction, and therefore the illumination angle is found which provides the best match between image and shaded GLD100 on the average.

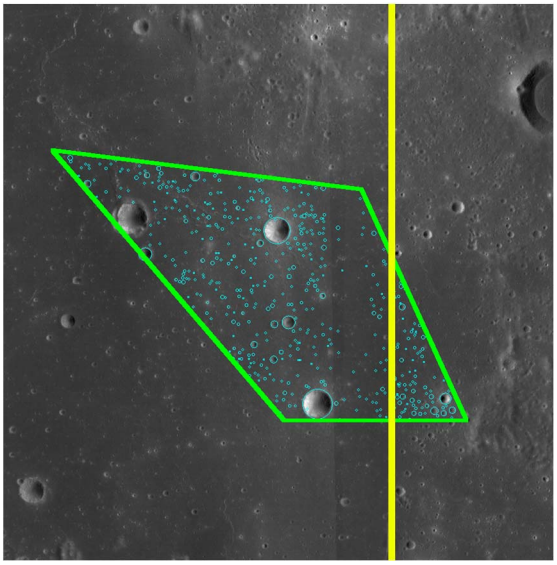

Fig. 5. Crater detections in area C3. The green polygon denots the study area and the blue line separates the two different illumination directions.

When illuminating the 3D crater models accordingly, many craters in the study area were not recognized. It is thus necessary to manually check for the actual illumination and whether the estimated illumination vector is correct or, if necessary, only a part of the image is used for the calculation of the illumination direction.

In the next step, the study areas in Oceanus Procellarum are again delineated by polygons. The optimal threshold value from Table I was applied to the areas P5, P41, P49, P50 and P51 in Oceanus Procellarum as defined in [6], resulting in the AMAs listed in Table III.

TABLE III. CDA-BASEDAND REFERENCE AMAS FOR THE STUDY AREAS IN OCEANUS PROCELLARUM, OBTAINED USING THE OPTIMAL DETECTION THRESHOLD INFERRED FROM AREAS C1-C5

Area	CDA-based AMA [Ga]			Reference AMA [Ga] [6]		
P49	1.71	-0.140	+0.110	2.01	-0.43	+0.37
P5	3.45	-0.019	+0.015	3.48	-0.06	+0.08
P41	3.33	-0.009	+0.009	2.13	-0.85	+0.75
P50	1.90	-0.166	+0.128	1.87	-0.25	+0.56
P51	2.01	-0.205	+0.166	1.85	-0.34	+0.37

It can be seen that all CDA-derived AMAs are very close to the manually manual crater count based reference AMAs from [6]. Similar to the region C3, an illumination change occurs in region P5 as shown in Fig. 6. The estimated AMA, however, does not differ much from the AMA given in [6].

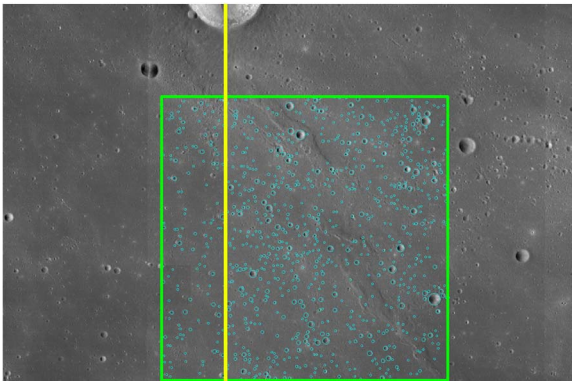

Fig. 6. Crater detections in area P5. The green polygon denotes the study area.

The largest deviations between CDA-based and reference AMAs occurs for regions P41 and P49 with reference AMAs of about 2 Ga, where the accuracy of CSFD-based AMA estimation in this age range is known to be low due to the low gradient of the production function [7]. Hence, these two areas P41 and P49 have relatively large errors of the reference AMA values in Table III. Despite the similarly large AMA estimation errors, the inferred AMAs of the regions P50 and P51 are in good agreement with the AMAs given in [6]. This implies that the AMA estimation is less sensitive to small errors for younger surfaces.

For all study regions except area P41, the deviations of the CDA-based AMA and the manual count based AMA are within the statistical error intervals. For AMAs between 2 and 3 Ga, the production function is almost horizontal [7], such that a small number of falsely detected or missed craters can make a large difference in AMA, hence ages in this range need to be interpreted with care.

VI. SUMMARY AND CONCLUSION

We adapted an automatic template matching based CDA to study areas in the lunar Mare Cognitum and calibrated it by adjusting the CDA's sensitivity threshold to match AMAs obtained in [6] for the same areas. Then we applied the calibrated CDA to another five study areas in lunar Oceanus

ISBN 978-0-9928626-7-1 © EURASIP 2017

Procellarum. The AMA has been computed for each of the ten study areas based on the obtained CDA-based CSFD. The automatically inferred AMAs were compared to the reference AMAs inferred from manual crater counts in [6].

The applied template matching method shows good agreement between CDA-based and manually inferred AMA with minor deviations. In most areas, the calculated age was within the one standard deviation error intervals. The CDA-based AMAs are reliable for surfaces older than 3.0 Ga or younger than 2.0 Ga, encouraging the application of CDAs as a valuable tool for planetary surface age estimation. In the range 2-3Ga, the error bars of the AMA are large due to an almost flat production function. It is thus suggested to be careful when using automatic CDAs on surfaces with ages in this range.

A disadvantage of the applied template matching method is that the illumination direction of the examined area needs to be known for each analyzed position in the image. If the regions do not show a uniform illumination, crater templates need to be generated for all occurring illumination conditions. This can be counteracted by (manually or automatically) detecting such variations and applying the CDA with the appropriate setting to each sub-region of homogeneous illumination.

To further improve the procedure, a combination of different automatic crater detectors could be used. This may provide a way to eliminate misdetections and achieve better detection results. Thus a larger amount of craters could be detected and a smaller amount of false detections would affect the AMA estimation.

Nevertheless, this relatively simple template-matching method has shown that it is applicable to crater detection on the Moon and thus in the future might also achieve good results on other planets, such as Mars or Pluto.

REFERENCES

[1] Neukum, Gerhard, Boris A. Ivanov, and William K. Hartmann. "Cratering records in the inner solar system in relation to the lunar reference system." Space Science Reviews 96, no. 1-4 (2001): 55-86.

[2] Salamuniccar, Goran, and Sven Loncaric. "Method for crater detection from Martian digital topography data using gradient value/orientation, morphometry, vote analysis, slip tuning, and calibration." IEEE transactions on Geoscience and Remote Sensing 48, no. 5 (2010): 2317-2329.

[3] Stepinski, T. F., Wei Ding, and R. Vilalta. "Detecting impact craters in planetary images using machine learning." Intelligent Data Analysis for Real-Life Applications: Theory and Practice. IGI Global, Hershey, PA (2012): 146-159.

[4] Schowengertdt, R. A. "Remote Sensing: Models and Methods for Image Processing", 3rd edition. Academic Press, 2007.

[5] Salamunićcar, Goran, and Sven Lončarić. "GT-57633 catalogue of Martian impact craters developed for evaluation of crater detection algorithms." *Planetary and Space Science* 56, no. 15 (2008): 1992-2008.

[6] Hiesinger, H., J. W. Head, U. Wolf, R. Jaumann, and G. Neukum. "Ages and stratigraphy of mare basalts in oceanus procellarum, mare nubium, mare cognitum, and mare insularum." Journal of Geophysical Research: Planets 108, no. E7 (2003).

[7] Neukum, Gerhard, Boris A. Ivanov, and William K. Hartmann. "Cratering records in the inner solar system in relation to the lunar reference system." Space Science Reviews 96.1-4 (2001): 55-86.

[8] Salih, A. L., M. Mühlbauer, A. Grumpe, J. H. Pasckert, C. Wöhler, and H. Hiesinger. "Mapping of Planetary Surface Age Based on Crater Statistics Obtained by AN Automatic Detection Algorithm." ISPRS-International Archives of the Photogrammetry, Remote Sensing and Spatial Information Sciences (2016): 479-486.

[9] R. V. Wagner, E. J. Speyerer, M. S. Robinson, and the LROC Team."New Mosaicked Data Products from the LROC Team", Proc. Lunar Planetary Science Conf. XXXXVI, abstract #1473, 2015.

[10] A. Grumpe und C. Wöhler; Generative Template-based Approach to the Automated Detection of Small Craters; EPSC Abstracts, 8; 2013.

[11] Smith, D. E. and 19 coauthors. "Initial observations from the Lunar Orbiter Laser Altimeter (LOLA)". Geophysical Research Letters 37, no. 18 (2010).

[12] Scholten, F., J. Oberst, K-D. Matz, T. Roatsch, M. Wählisch, E. J. Speyerer, and M. S. Robinson. "GLD100: The near-global lunar 100 m raster DTM from LROC WAC stereo image data." Journal of Geophysical Research: Planets 117, no. E12 (2012).

[13] Hapke, Bruce. "Bidirectional reflectance spectroscopy: 5. The coherent backscatter opposition effect and anisotropic scattering." Icarus 157, no. 2 (2002): 523-534.

[14] Hapke, Bruce. Theory of reflectance and emittance spectroscopy. Cambridge University Press, 2012.

ISBN 978-0-9928626-7-1 © EURASIP 2017